

pubs.acs.org/crystal Article

Shaping Organic Microcrystals Using Focused Ion Beam Milling

Published as part of a Crystal Growth and Design virtual special issue Remembering the Contributions and Life of Prof. Joel Bernstein

Wangxiang Li, Jeremiah van Baren, Adam Berges, Elena Bekyarova, Chun Hung Lui, and Christopher J. Bardeen*



Cite This: Cryst. Growth Des. 2020, 20, 1583-1589



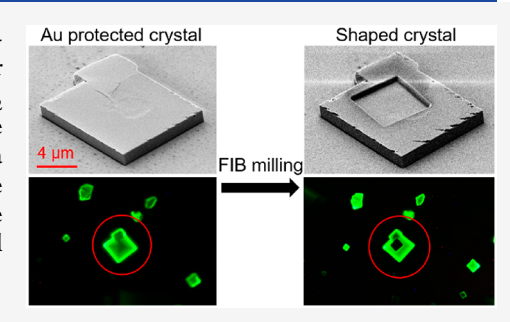
ACCESS

Metrics & More

Article Recommendations

s Supporting Information

ABSTRACT: The technique of focused ion beam (FIB) milling is used to cut two-dimensional shapes into single crystals composed of the organic semiconductor molecule perylene. The use of an ultrathin Au coating and its removal using a $\rm KI/I_2$ etchant solution allow the crystal to be imaged in the FIB apparatus while protecting it from electron beam damage. Using this approach, features with a spatial resolution on the order of 130 nm can be created while retaining 90% of the original photoluminescence intensity in the surrounding crystal regions. These proof-of-principle experiments demonstrate that FIB milling could provide a general way to control the nanoscale morphology of organic molecular crystals.



■ INTRODUCTION

Molecular crystals are most commonly used in science for structure determination via X-ray or electron diffraction techniques. However, organic crystals are starting to attract attention as functional materials in their own right. The molecular ordering and lack of grain boundaries in a single crystal can lead to very high charge and exciton mobilities, making them attractive candidates for field-effect transistors and photovoltaic cells. 1-4 The unique mechanical properties of molecular crystals have also attracted attention, especially their ability to utilize thermal or photoinduced phase transitions to generate mechanical work or motion. 5,6 In the emerging field of functional molecular crystals, there are several levels of material engineering that need to be considered. First, there is the molecule itself, whose properties can be tuned using the methods of chemical synthesis. Second, the molecular packing can be modified using the tools of crystal engineering. Third, the morphology (size, shape, and orientation) of the crystal can be modified. This last phase of control is necessary for the incorporation of single crystals into practical devices but has proven challenging. Crystal growth is controlled by noncovalent self-assembly processes that are sensitive to both molecular-scale phenomena (nucleation and molecular interactions) and larger scale phenomena such as mass transport and crystal-substrate attachment.

In order to gain some degree of control over molecular crystal shape, most workers adopt a "bottom-up" strategy in which environmental factors are used to influence the self-assembly process. These strategies include modifying solvent and surfactant growth conditions, 7-10 surface functionalization, 11-14 templated growth, 15-17 or the use of highly

nonequilibrium conditions such as laser guided growth. $^{18-20}$ All of these approaches have met with some success, but the field has yet to identify a general method that can guide molecules to self-assemble into a predetermined shape. In many cases, a relatively broad distribution of crystal sizes and orientations is obtained, and the crystals often retain their intrinsic habit, e.g., rectangular prisms, needles, or plates. Meanwhile, the inorganic community often utilizes "top-down" subtractive methods to generate arbitrary shapes in materials such as silicon. Electron and photon-based lithography techniques utilize patterned illumination and etching to selectively remove sections of the parent crystal, leaving only the desired shape. More recently, focused ion beam (FIB) milling has been used to physically abrade away selected regions of the starting crystal.^{21–24} Both electron beam lithography²⁵ and FIB milling²⁶ have the ability to create user-defined features on sub-10 nm length scales.

Given the advanced state of "top-down" nanofabrication techniques, we became interested in whether they could be applied to the problem of shape control in molecular crystals. Electron lithography and photolithography typically require coating the crystal with a resist polymer that can be patterned and redissolved. This strategy is difficult to implement with molecular crystals due to solubility constraints: the same solvent used to deposit the resist may also dissolve the crystal,

Received: October 7, 2019 Revised: February 6, 2020 Published: February 6, 2020



leading to a mixed interfacial layer or loss crystallinity. FIB milling, on the other hand, utilizes the direct impact of ions to knock out material, without the need for intermediate chemical steps such as polymer spin-coating or reactive etching. The operator can visualize the object in real time using electron microscopy in order to direct the milling beam. This method can in principle bypass chemical compatibility issues. However, there are several challenges in applying it to organic materials. First, most organic solids are insulators, so using electron microscopy to align and visualize the object during the milling process presents a challenge. Second, organic materials are prone to damage by energetic charged particles, both the electrons used for imaging and the atomic ions used for cutting. Third, a considerable amount of heat can be deposited by the energetic ions, which can induce melting or other phase changes in soft materials such as organic crystals and polymers. These practical difficulties may explain the scarcity of FIBmilling results on organic solids. Although it has been used to cut patterns into a variety of polymers^{27–30} and photonic structures into perovskite crystals,^{31,32} so far there has been no report of using FIB-milling to shape an organic molecular crystal.

In this paper, we explore the use of FIB-milling to cut arbitrary two-dimensional shapes into crystal plates of the organic semiconductor molecule perylene (PER). The key step is the application of an ultrathin gold coating that protects the crystal during ion exposure, followed by a KI/I₂ Au removal step that does not harm the organic. Using the FIB, we are able to completely remove selected portions of a single crystal, as well as write submicron features into single crystals. These proof-of-principle experiments represent an encouraging first step in the use of FIB-milling to create molecular crystals with user-defined shapes that could enable systematic studies of how crystal morphology affects function.

■ EXPERIMENTAL SECTION

Preparation of Perylene Microcrystals. A concentrated PER/toluene solution (10^{-3} M) was drop-cast onto a clean glass substrate and dried in air, forming a yellow film composed of individual microcrystals. A 4 nm Au conductive layer was coated onto the substrate using electron beam evaporation (Temescal BJD 1800 system). The sample was then mounted in a Leo XB 1540 focused ion beam milling system (Zeiss).

Micromachining of Perylene Crystal. The target crystal was first located and imaged by the scanning electron microscopy inside the FIB system. The desired milling patterns were designed during the imaging process using the shape function of SmartSEM software. The milling parameters were also set before switching to FIB imaging in order to minimize premilling exposure to the Ga+ ion beam. After switching to FIB mode, the magnification was set to the same as the SEM magnification. Typically, a slight realignment between the design pattern and the target crystal is needed, after which the sample can be milled by the Ga+ ion beam. The parameters of FIB imaging and milling are identical (30 kV, 50 pA) in order to avoid changing the aperture, which will induce a shift of the beam alignment. The time of milling for each crystal was estimated from the empirical perylene etching rate of 800 s/ μ m³. After milling, the Au coating layer was removed by immersing the sample in a commercial potassium iodide/ iodine etchant (Transene Gold Etchant TFA) for 2 s at room temperature, immediately followed by water rinsing.

Microscopy. Optical images were acquired using an Olympus BX51WI microscope. Fluorescence images were taken through a fluorescein isothiocyanate (FITC) filter. AFM images were collected using a Digital Instruments Nanoscope IIIA scanned probe microscope system (AFM Probe: NSG01, NT-MDT Spectrum Instruments) in tapping mode.

Photoluminescence Spectroscopy. Photoluminescence (PL) spectra from localized regions in a single crystal were collected using a Nicolet Almega XR dispersive Raman microscope using 532 nm laser excitation with an estimated focus size of 1 µm. Time-resolved PL experiments were conducted using the time-correlated single photon counting technique. For the high repetition rate experiments, samples were excited with 515 nm light generated by the second harmonic of a 1030 nm (Light Conversion Inc., Pharos) laser with an 80 MHz repetition rate and a 90 fs pulse duration. These samples were first located through the integrated microscope system with a 40× objective (NA = 0.6) before excitation. The PL signal was detected with an avalanche photodiode (PicoQuant, PDM), and its temporal trace was measured by time-correlated single photon counting (PicoQuant, PicoHarp 300). For the lower repetition rate experiments, samples were excited with 400 nm light generated by the second harmonic of a mode-locked 800 nm (Coherent, Inc., Libra) Ti:sapphire laser with a 1 kHz repetition rate and a 100 fs pulse duration. Samples were located and excited as previously described, with the PL signal and its temporal trace measured collected by a streak camera and triggering unit (Hamamatsu Photonics, C4334 and C4792-01).

RESULTS AND DISCUSSION

We chose the α -polymorph of crystalline PER as a model molecular crystal system to demonstrate the FIB-milling approach. PER is a polyaromatic hydrocarbon whose core structure has been used as the basis for molecules with applications as electron acceptors in solar cells, singlet fission chromophores, field effect transistors, and organic lightemitting diodes.³³ Its melting point is 255 °C, and the crystal also sublimes at moderate temperatures, so it is representative of the typical challenges that will be encountered for organic molecular crystals. Another advantage of PER crystals is their strong photoluminescence (PL) that arises from excimers that form in the α -polymorph. ^{34–36} This PL signal provides a facile way to characterize the crystal and assess damage and/or phase changes. The α -polymorph of PER grows in distinctive square or diamond shaped plates, ideal for testing two-dimensional (2D) FIB-milling techniques. The size and thickness of these plates depend on growth conditions. For the solvent evaporation method used here, the plates were typically 5-10 μ m wide and 200–2000 nm thick.

As mentioned in the Introduction, it is impossible to directly image a molecular crystal inside a FIB-milling apparatus due to rapid charge accumulation in the poorly conducting organic. Our goal was to encapsulate the crystal under a conductive coating that was either transparent or could be easily removed. We first tried graphene as an encapsulating layer, as this 2D material can provide sufficient surface conductivity for SEM imaging while not perturbing the underlying crystal.³⁷ Unfortunately, even at the lowest electron beam energies, exposure to the electron imaging beam during the alignment and positioning procedure led to a loss of PL intensity of 80% or more in the absence of milling. In order to provide more protection for the crystal, we turned to an electron-beam evaporated Au coating. We found that a 4 nm Au layer preserved more than 90% of the crystal's original PL signal (see below) while providing sufficient surface conductivity to obtain high resolution SEM images.

After Au coating, the crystal was placed in the FIB-SEM system and scanned using an electron beam. Once the target crystal was located by SEM imaging, a directional beam of high energy Ga⁺ ions was used to remove sections of the crystal. The voltage was kept as low as possible to avoid potential damage from ions deflected into nontarget areas of the crystal.

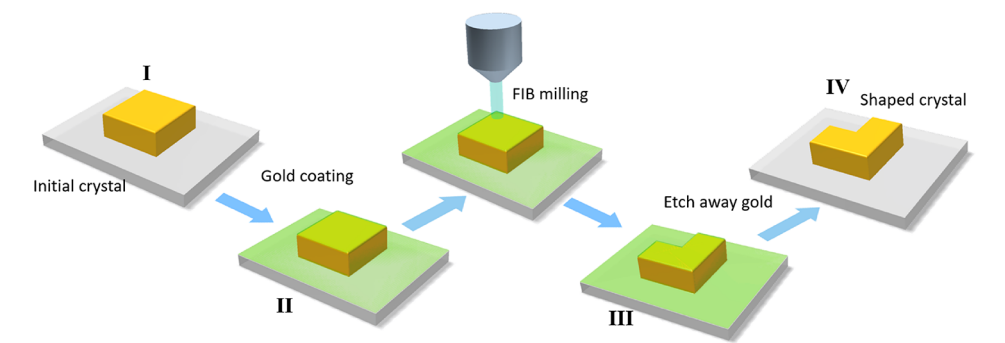


Figure 1. Schematic illustration of the FIB micromachining process for molecular crystals. The PER crystal (I) is first coated with a 4 nm thick gold layer (shown as a green translucent coating). The coated sample (II) is mounted in the FIB chamber and milled into the designed shape. After milling, the shaped crystal (III) is dipped into a KI/I_2 etching solution to remove the gold layer. After rinsing with water, the shaped crystal (IV) is allowed to dry before characterization.

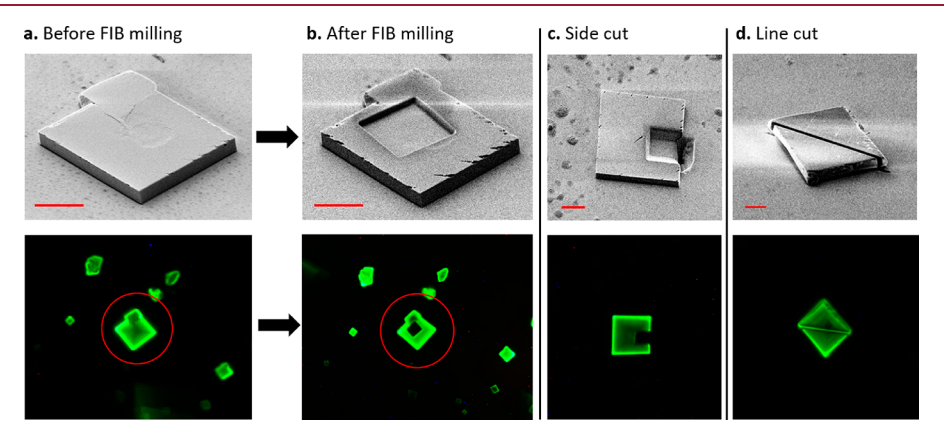


Figure 2. SEM (top) and fluorescence (bottom) images of FIB-milled PER crystals. A single PER crystal before (a) and after (b) FIB-milling of a square in the center of the crystal, resulting in a frame structure. (c) a PER crystal with a rectangular cut on the side that extends into the substrate, (d) a square crystal cut into two triangles. For all SEM images, the scale bar = 4 μ m. The crystals in the fluorescence image are the same crystals in the SEM images above.

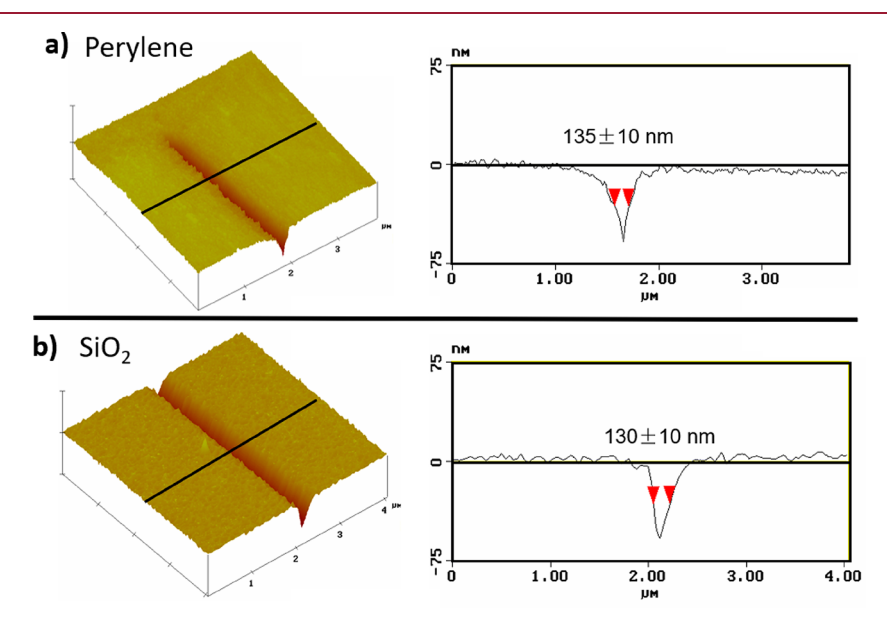


Figure 3. AFM surface scans of (a) a PER crystal and (b) a SiO₂ substrate after a single cut using the FIB. For both images, the cross-section of the cut can be extracted, leading to similar full-width-half-maximum values of 135 ± 10 nm and 130 ± 10 nm for the two substrates.

We empirically found an etching rate of ${\sim}800~\text{s}/{\mu}\text{m}^3$, given a 50 pA ion beam at 30 kV. Lower voltages resulted in an unacceptably low milling rate. After the milling process was complete, the shaped crystals could be reimaged using SEM to

confirm the desired shape. Finally, the crystal was removed from the FIB apparatus, and the protective Au layer was dissolved using a commercial etching solution. Although Aqua Regia is the most commonly used etchant to remove Au, this

strong oxidant would also react with the underlying organic. Instead, we used a commercial iodine-based etchant that left the organic intact. The entire process is schematically illustrated in Figure 1.

In Figure 2, we show some examples of FIB-milled PER crystals. The first two images show a microplate before (a) and after (b) the excision of a square region inside the plate. Figure 2c shows a crystal after a square has been milled out of the side. Note that the milled region extends past the crystal, and so some of the glass substrate was also removed, leaving a pit adjacent to the target crystal. In Figure 2d, we show a square plate that has been cut in half by the FIB. Note that in all the fluorescence images, the edges of the crystals typically appear brighter than the interior regions. This is because PL that is emitted below the critical angle is trapped within the highindex crystal and waveguided to the edges, where it is scattered out.³⁸ The resolution of the cutting can be assessed by measuring the full-width-half-maximum (fwhm) and depth of a single line drawn across a crystal face. Figure 3a shows a single cut across a PER crystal (fwhm = 135 ± 10 nm), while Figure 3b shows one across a silicon dioxide surface (fwhm = 130 \pm 10 nm). Both cuts have the same average depth of 40 nm. The FIB milling parameters for PER and silicon dioxide are the same to within the error, so it does not appear that softening of the organic limits the resolution of the milling, at least on the 100 nm length scale. Optimization of the crystal thickness and FIB parameters would hopefully reduce this width well below 100 nm.

The shapes in Figure 2 rely on the complete removal of the crystal in specified regions along orthogonal directions. The FIB can also be programmed to cut more complex shapes with specified depths, rather than cutting completely through the crystal. To illustrate this capability, we programmed the FIB to remove material and leave the letter Y inside a 10 \times 10 μ m square PER crystal with a thickness of 2 μ m. The Y-shape is analogous to a planar waveguide optical splitter structure used in photonic circuits. The cutting speed parameters were adjusted to only remove the top 20 nm of crystal in a square around the Y shape. Figure 4a shows an SEM image of the

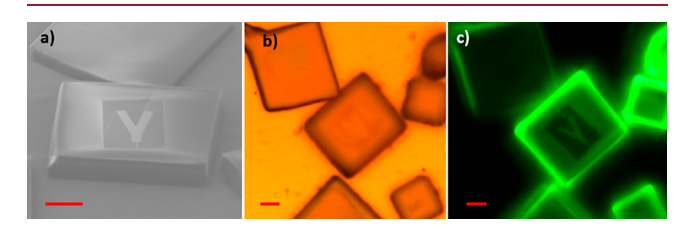


Figure 4. (a) SEM image of a Y shape imprinted onto the surface of a PER crystal, with the surrounding material removed to a depth of 20 nm. Transmission (b) and fluorescence (c) microscopy images of the same crystal. For all images, the scale bar = $4 \mu m$.

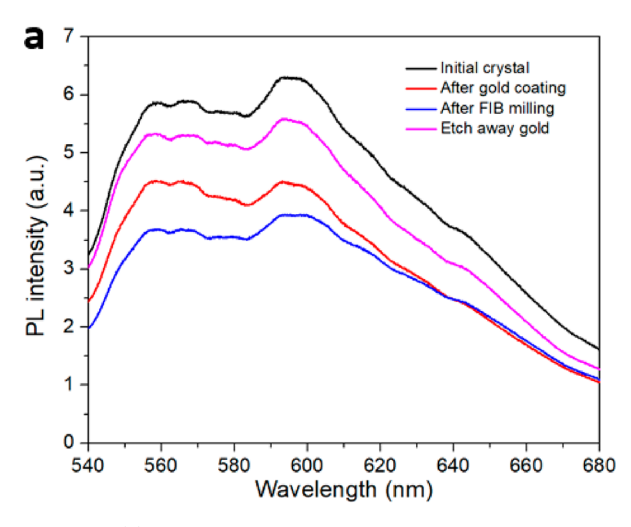
outcome of this procedure, with the Y clearly imprinted in a square well cut in the interior of the larger crystal. This Y shape resides on top of the rest of the crystal, while the underlying PER foundation remains intact. This can be clearly seen in the optical microscopy image in Figure 4b, where the Y is barely visible on top of the yellow-orange crystal. The contrast becomes more pronounced in the fluorescence microscopy image in Figure 4c, where the Y emits green fluorescence while the underlying square that has been milled is dark. This dark background indicates that the exposed regions of the crystal experience significant PL quenching, even though the SEM and

transmitted light microcopy images show that the underlying PER crystal is still intact. This is not surprising, since once the protective Au coating has been milled away, the organic will be exposed to high energy ions that are known to introduce both chemical and physical defects in polymers. ^{40–42} A comparison of the roughness of the PER crystal surface before and after exposure to the milling beam showed a slight increase in mean roughness, from 0.6 to 1.2 nm (Supporting Information, Figure S4), which may also be indicative of damage.

One important question is whether the regions of the crystal that are not directly exposed to the milling beam also sustain damage. In Figures 2 and 4, the crystal regions that have not been exposed to the ion beam appear to retain their full PL intensity, but we wanted to check this quantitatively. We used a confocal microscope to collect PL spectra from specific regions of a single crystal located 2-4 µm away from the milled region. In Figure 5a, we show the PL spectrum of a single crystal taken at various points during the procedure shown in Figure 1. All four spectra share the same broad shape characteristic of the α -PER excimer. Figure 5b shows that the integrated PL intensity drops by 40% after the 4 nm Au layer is applied. This semitransparent layer can quench the excimer both through nonradiative energy transfer and by absorbing/ reflecting the radiated photons. After milling, the PL signal dropped again by about 10%. However, this decrease could be due to the loss of material as well as chemical damage from the milling process. After removal of the Au, the PL recovered to 90% of the original level. Thus, the overall loss of PL due to the milling procedure was about 10%. Experiments on other crystals consistently yielded an 8-12% decrease in the PL intensity.

The PL decays of a crystal before and after the FIB-milling procedure had similar shapes, as shown in Figure 6. The decays are biexponential, of the form $Ae^{-t/\tau_A} + Be^{-t/\tau_B}$, and the lifetimes and pre-exponential factors are summarized in Table 1. The average lifetime, given by $\frac{A\tau_A + B\tau_B}{A + B}$, is proportional to the integrated fluorescence intensity and decreases from 2.17 to 1.87 ns. This 13% decrease is close to the 10% decrease in steady-state intensity shown in Figure 5. Both the short and long decay times decrease in the exposed sample, consistent with quenching of the mobile excimer states by defects in the PER crystal. If the loss of PL intensity was merely due to the loss of material, with the surrounding PER crystal unaffected, then we would expect to see the same excimer lifetime from the exposed and unexposed portions. We note that the average PL lifetime of the PER crystals reported here is shorter than that reported by us previously,³⁷ which we attribute to the use of a high repetition rate laser for these microscopy measurements. The high repetition rate and small spot size can lead to localized heating of the crystal, which will accelerate the PL decay. We confirmed that when bulk measurements were done on the same crystals at a lower repetition rate (1 kHz) we obtained longer decays (Supporting Information, Figure S3) consistent with our earlier paper.

The loss of PL intensity in the surrounding crystal regions may originate from several factors. For example, the I_2 in the etching solution may be incorporated into the PER crystal and lead to doping. We tested for this possibility by exposing the crystals to the etching solution in the absence of Au coating or ion exposure. No measurable drop in PL intensity was observed for these samples (Supporting Information, Figure S1). However, if the crystals were coated with Au and then



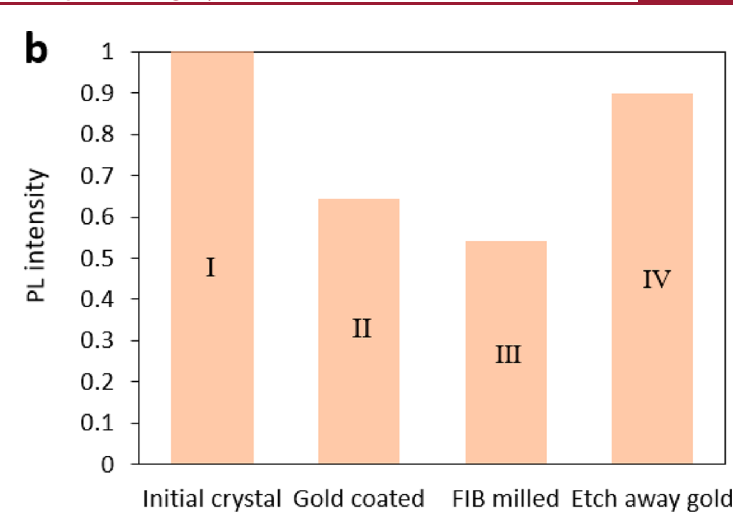


Figure 5. (a) PL spectrum of a PER crystal at each step given in Figure 1. All the spectra are collected from a spot located within 2–4 μ m of the FIB milling area. (b) Comparison of the integrated PL intensity at each step given in Figure 1, normalized to that measured at step I. After Au coating and FIB-milling, the PL intensity decreases by about 45%, but it recovers to 90% of its original value after the Au layer is etched away.

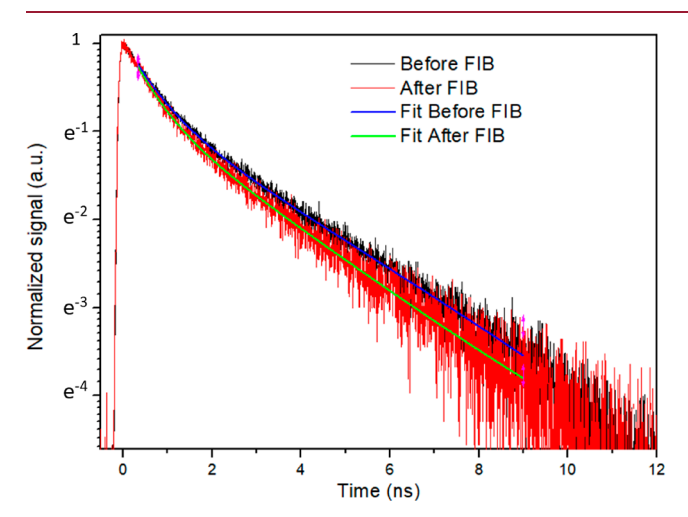


Figure 6. PL decays with biexponential fits before (black) and after (red) the PER crystal undergoes the FIB shaping process. After FIB milling, the average PL lifetime decreases slightly.

Table 1. Lifetimes and Pre-exponential Factors Used to Fit the PL Decays

$Ae^{-t/\tau_A} + Be^{-t/\tau_B}$	A	$\tau_{\rm A}~({\rm ns})$	В	$\tau_{\rm B}~({\rm ns})$	$ au_{ ext{average}}$ (ns)
before FIB	0.463	3.220	0.326	0.697	2.17
after FIB	0.449	2.730	0.301	0.588	1.87

etched away without exposure to FIB milling, a 5% drop in PL was observed (Supporting Information, Figure S2). This result suggests that half of the observed PL loss can be attributed to effects from the coating itself, possibly due to diffusion of Au atoms into the organic phase. The other 5% PL loss is presumably due to ion exposure during the FIB procedure. The process of locating and aligning the sample with the SEM/FIB beam causes the entire crystal to be exposed to charged particles, some of which penetrate the Au coating. Both of these sources of damage can be reduced by further optimization of the procedure. A thicker Au coating and more efficient alignment procedure should reduce the exposure of the organic to ions. Extending the etching period or heating the crystal may facilitate removal of Au atoms. However, the

retention of 90% of the PL already represents an improvement relative to the 70% PL retention seen in perovskite thin films that are processed using gas-assisted FIB milling, and we did not make a systematic effort to improve the PL retention for this study. Finally, we should emphasize that a PL decrease of 10% does not necessarily mean that 10% of the crystal has been destroyed. Efficient energy migration in molecular crystals can amplify the effect of even low density defects, leading to a substantial loss of PL. $^{46-48}$

CONCLUSION

The results in this article show that it is possible to apply the techniques of FIB-milling to shape molecular crystals. The use of an ultrathin Au coating and its removal using a KI/I₂ etchant provide a gentle way to prepare the crystal for imaging in the FIB apparatus while protecting it from electron beam damage. Using this approach, we have milled features with a spatial resolution on the order of 130 nm while retaining 90% of the original PL intensity in the unmilled regions of the crystal. Even smaller features should be possible using more advanced FIB techniques and thinner crystals. While the top-down FIB method is not practical for mass-producing shaped microcrystals, it provides a new capability to create complex shapes in single crystals with high spatial resolution. This capability can enable the exploration of how variations in crystal shape lead to different optical, electronic, and mechanical properties. These insights can then guide the design of new materials that incorporate molecular crystal elements, for example, waveguides or photomechanical actuators.

ASSOCIATED CONTENT

Supporting Information

The Supporting Information is available free of charge at https://pubs.acs.org/doi/10.1021/acs.cgd.9b01327.

PL intensity data of PER on the effect of gold etchant and gold coating; PL decay of PER excited by a 1 kHz laser; roughness analyses of PER surface before and after FIB milling (PDF)

AUTHOR INFORMATION

Corresponding Author

Christopher J. Bardeen — Department of Chemistry, University of California, Riverside, Riverside, California 92521, United States; Orcid.org/0000-0002-5755-9476; Email: christopher.bardeen@ucr.edu

Authors

Wangxiang Li — Department of Chemistry, University of California, Riverside, Riverside, California 92521, United States Jeremiah van Baren — Department of Physics, University of California, Riverside, Riverside, California 92521, United States Adam Berges — Department of Chemistry, University of California, Riverside, Riverside, California 92521, United States Elena Bekyarova — Department of Chemistry, University of California, Riverside, Riverside, California 92521, United States; ⊚ orcid.org/0000-0001-7565-2773

Chun Hung Lui – Department of Physics, University of California, Riverside, Riverside, California 92521, United States

Complete contact information is available at: https://pubs.acs.org/10.1021/acs.cgd.9b01327

Notes

The authors declare no competing financial interest.

ACKNOWLEDGMENTS

This work was supported by the National Science Foundation Grant CHE-1800187.

REFERENCES

- (1) Reese, C.; Bao, Z. Organic Single Crystal Field-Effect Transistors. *Mater. Today* **2007**, *10*, 20–27.
- (2) Najafov, H.; Lee, B.; Zhou, Q.; Feldman, L. C.; Podzorov, V. Observation of Long-range Exciton Diffusion in Highly Ordered Organic Semiconductors. *Nat. Mater.* **2010**, *9*, 938–943.
- (3) Podzorov, V. Organic Single Crystals: Addressing the Fundamentals of Organic Electronics. MRS Bull. 2013, 38, 15–24.
- (4) Karak, S.; Lim, J. A.; Ferdous, S.; Duzhko, V. V.; Briseno, A. L. Photovoltaic Effect at the Schottky Interface with Organic Single Crystal Rubrene. *Adv. Funct. Mater.* **2014**, 24, 1039–1046.
- (5) Kim, T.; Zhu, L.; Al-Kaysi, R. O.; Bardeen, C. J. Organic photomechanical materials. *ChemPhysChem* **2014**, *15*, 400–414.
- (6) Naumov, P.; Chizhik, S.; Panda, M. K.; Nath, N. K.; Boldyreva, E. Mechanically Responsive Molecular Crystals. *Chem. Rev.* **2015**, 115, 12440–12490.
- (7) Zhang, X.; Dong, C.; Zapien, J. A.; Ismathullakhan, S.; Kang, Z.; Jie, J.; Zhang, X.; Chang, J. C.; Lee, C.-S.; Lee, S.-T. Polyhedral Organic Microcrystals: From Cubes to Rhombic Dodecahedra. *Angew. Chem., Int. Ed.* **2009**, 48, 9121–9123.
- (8) Lin, Z.-Q.; Sun, P.-J.; Tay, Y.-Y.; Liang, J.; Liu, Y.; Shi, N.-E.; Xie, L.-H.; Yi, M.-D.; Qian, Y.; Fan, Q.-L.; Zhang, H.; Hng, H. H.; Ma, J.; Zhang, Q.; Huang, W. Kinetically Controlled Assembly of a Spirocyclic Aromatic Hydrocarbon into Polyhedral Micro/Nanocrystals. ACS Nano 2012, 6, 5309—5319.
- (9) Al-Kaysi, R. O.; Zhu, L.; Al-Haidar, M.; Al-Muhannah, M. K.; El-Boubbou, K.; Hamdan, T. M.; Bardeen, C. J. Chemical reaction method for growing photomechanical organic microcrystals. *CrystEngComm* **2015**, *17*, 8835–8842.
- (10) Peng, L.; Chen, Y.-N.; Dong, Y. Q.; He, C.; Wang, H. Surfactant-Assisted Self-Assembled Polymorphs of AIEgen Di(4-propoxyphenyl)dibenzofulvene. *J. Mater. Chem. C* **2017**, *5*, 557–565.
- (11) Briseno, A. L.; Mannsfeld, S. C. B.; Ling, M. M.; Liu, S.; Tseng, R. J.; Reese, C.; Roberts, M. E.; Yang, Y.; Wudl, F.; Bao, Z. Patterning organic single-crystal transistor arrays. *Nature* **2006**, 444, 913–917.

- (12) Schiek, M.; Balzer, F.; Al-Shamery, K.; Brewer, J. R.; Lutzen, A.; Rubahn, H. G. Organic molecular nanotechnology. *Small* **2008**, *4*, 176–181.
- (13) Wilkinson, F. S.; Norwood, R. F.; McLellan, J. M.; Lawson, L. R.; Patrick, D. L. Engineered growth of organic crystalline films using liquid crystal solvents. *J. Am. Chem. Soc.* **2006**, *128*, 16468–16469.
- (14) Minemawari, H.; Yamada, T.; Matsui, H.; Tsutsumi, J.; Haas, S.; Chiba, R.; Kumai, R.; Hasegawa, T. Inkjet printing of single-crystal films. *Nature* **2011**, *475*, 364–367.
- (15) Ha, J.-M.; Wolf, J. H.; Hillmyer, M. A.; Ward, M. D. Polymorph Selectivity under Nanoscopic Confinement. *J. Am. Chem. Soc.* **2004**, *126*, 3382–3383.
- (16) Jiang, Q.; Ward, M. D. Crystallization under Nanoscale Confinement. Chem. Soc. Rev. 2014, 43, 2066–2079.
- (17) Al-Kaysi, R. O.; Bardeen, C. J. General Method for the Synthesis of Crystalline Organic Nanorods using Porous Alumina Templates. *Chem. Commun.* **2006**, 1224–1226.
- (18) Balzer, F.; Rubahn, H. G. Laser-controlled Growth of Needleshaped Organic Nanoaggregates. *Nano Lett.* **2002**, *2*, 747–750.
- (19) Okutsu, T.; Nakamura, K.; Haneda, H.; Hiratsuka, H. Laser-Induced Crystal Growth and Morphology Control of Benzopinacol Produced from Benzophenone in Ethanol/Water Mixed Solution. *Cryst. Growth Des.* **2004**, *4*, 113–115.
- (20) Sugiyama, T.; Masuhara, H. Laser-Induced Crystallization and Crystal Growth. *Chem. Asian J.* **2011**, *6*, 2878–2889.
- (21) Giannuzzi, L. A.; Stevie, F. A. A Review of Focused Ion Beam Milling Techniques for TEM Specimen Preparation. *Micron* **1999**, *30*, 197–204.
- (22) Tseng, A. A. Recent Developments in Nanofabrication Using Focused Ion Beams. *Small* **2005**, 1, 924–939.
- (23) Special Issue on Focused Ion Beam Microscopy and Micromachining. MRS Bull. 2007, 32.389
- (24) Rajput, N. S.; Luo, X. FIB Micro-/Nano-Fabrication. In *Micro and Nano Technologies, Micromanufacturing Engineering and Technology*; Qin, Y., Ed.; William Andrew Publishing: London, 2015; pp 61–80
- (25) Manfrinato, V. R.; Zhang, L.; Su, D.; Duan, H.; Hobbs, R. G.; Stach, E. A.; Berggren, K. K. Resolution Limits of Electron-Beam Lithography toward the Atomic Scale. *Nano Lett.* **2013**, *13*, 1555–1558
- (26) Menard, L. D.; Ramsey, J. M. Fabrication of Sub-5 nm Nanochannels in Insulating Substrates Using Focused Ion Beam Milling. *Nano Lett.* **2011**, *11*, 512–517.
- (27) Niihara, K.-i.; Kaneko, T.; Suzuki, T.; Sato, Y.; Nishioka, H.; Nishikawa, Y.; Nishi, T.; Jinnai, H. Nanoprocessing and Nanofabrication of a Structured Polymer Film by the Focused-Ion-Beam Technique. *Macromolecules* **2005**, *38*, 3048–3050.
- (28) Guan, L.; Peng, K.; Yang, Y.; Qiu, X.; Wang, C. The Nanofabrication of Polydimethylsiloxane Using a Focused Ion Beam. *Nanotechnology* **2009**, *20*, 145301.
- (29) Kochumalayil, J. J.; Meiser, A.; Soldera, F.; Possart, W. Focused Ion Beam Irradiation Morphological and Chemical Evolution in PMMA. *Surf. Interface Anal.* **2009**, *41*, 412–420.
- (30) Lee, C. C.; Proust, G.; Alici, G.; Spinks, G. M.; Cairney, J. M. Three-Dimensional Nanofabrication of Polystyrene by Focused Ion Beam. *J. Microsc.* **2012**, 248, 129–139.
- (31) Alias, M. S.; Dursun, I.; Shi, D.; Saidaminov, M. I.; Diallo, E. M.; Priante, D.; Ng, T. K.; Bakr, O. M.; Ooi, B. S. Focused-Ion Beam Patterning of Organolead Trihalide Perovskite for Subwavelength Grating Nanophotonic Applications. J. Vac. Sci. Technol., B: Nanotechnol. Microelectron.: Mater., Process., Meas., Phenom. 2015, 33, No. 051207.
- (32) Alias, M. S.; Yang, Y.; Ng, T. K.; Dursun, I.; Shi, D.; Saidaminov, M. I.; Priante, D.; Bakr, O. M.; Ooi, B. S. Enhanced Etching, Surface Damage Recovery, and Submicron Patterning of Hybrid Perovskites using a Chemically Gas-Assisted Focused-Ion Beam for Subwavelength Grating Photonic Applications. *J. Phys. Chem. Lett.* **2016**, *7*, 137–142.

- (33) Zhan, X.; Facchetti, A.; Barlow, S.; Marks, T. J.; Ratner, M. A.; Wasielewski, M. R.; Marder, S. R. Rylene and Related Diimides for Organic Electronics. *Adv. Mater.* **2011**, 23, 268–284.
- (34) Walker, B.; Port, H.; Wolf, H. C. The Two-Step Excimer Formation in Perylene Crystals. *Chem. Phys.* **1985**, 92, 177–185.
- (35) Fujino, T.; Tahara, T. Femtosecond Fluorescence Up-Conversion Microscopy: Exciton Dynamics in α -Perylene Microcrystal. *J. Phys. Chem. B* **2003**, *107*, 5120–5122.
- (36) Pick, A.; Klues, M.; Rinn, A.; Harms, K.; Chatterjee, S.; Witte, G. Polymorph-Selective Preparation and Structural Characterization of Perylene Single Crystals. *Cryst. Growth Des.* **2015**, *15*, 5495–5504.
- (37) Li, W.; Tierce, N. T.; Bekyarova, E.; Bardeen, C. J. Protection of Molecular Microcrystals by Encapsulation under Single-Layer Graphene. ACS Omega 2018, 3, 8129–8134.
- (38) Takazawa, K. Understanding the Emission Pattern Produced by Focused Laser Beam Excitation of Perylene Square Single Crystals. *Chem. Phys. Lett.* **2017**, *667*, 284–289.
- (39) Prajzler, V.; Maštera, R.; Špirková, J.; Jeřábek, V. Compact Multimode Polymer Optical 1 × 2 Y Splitters with Large Core Planar Waveguide. *J. Optics* **2014**, *43*, 310–316.
- (40) Kim, S.; Jeong Park, M.; Balsara, N. P.; Liu, G.; Minor, A. M. Minimization of Focused Ion Beam Damage in Nanostructured Polymer Thin Films. *Ultramicroscopy* **2011**, *111*, 191–199.
- (41) Allen, F. I.; Velez, N. R.; Thayer, R. C.; Patel, N. H.; Jones, M. A.; Meyers, G. F.; Minor, A. M. Gallium, Neon and Helium Focused Ion Beam Milling of Thin Films Demonstrated for Polymeric Materials: Study of Implantation Artifacts. *Nanoscale* **2019**, *11*, 1403–1409.
- (42) Orthacker, A.; Schmied, R.; Chernev, B.; Froch, J. E.; Winkler, R.; Hobisch, J.; Trimmel, G.; Plank, H. Chemical Degradation and Morphological Instabilities During Focused Ion Beam Prototyping of Polymers. *Phys. Chem. Chem. Phys.* **2014**, *16*, 1658–1666.
- (43) Uchida, T.; Akamatu, H. Organic Semiconductors with High Conductivity. III. Perylene-Iodine Complex. *Bull. Chem. Soc. Jpn.* **1961**, 34, 1015–1020.
- (44) Yao, Y.; Peng, S.-a.; Huang, X.-n.; Zhang, D.-y.; Shi, J.-y.; Jin, Z. A Uniform Stable P-type Graphene Doping Method with a Gold Etching Process. *Nanotechnology* **2019**, *30*, 405205.
- (45) Cho, J. H.; Kim, D. H.; Jang, Y.; Lee, W. H.; Ihm, K.; Han, J.-H.; Chung, Su.; Cho, K. Effects of Metal Penetration into Organic Semiconductors on the Electrical Properties of Organic Thin Film Transistors. *Appl. Phys. Lett.* **2006**, *89*, 132101.
- (46) Powell, R. C.; Soos, Z. G. Singlet exciton energy transfer in organic solids. *J. Lumin.* 1975, 11, 1–45.
- (47) Tomura, M.; Takahashi, Y. Migration of Excimer Energy in Pyrene Crystal. J. Phys. Soc. Jpn. 1971, 31, 797–801.
- (48) Gregg, B. A.; Sprague, J.; Peterson, M. W. Long-Rangle Singlet Energy Transfer in Perylene Bis(phenethylimide) Films. *J. Phys. Chem. B* 1997, 101, 5362–5369.